O. Kostyuk[1,2], Ya. Yavorsky[1], B. Dzundza[1], Z. Dashevsky[3]

# Development of Thermal Detector Based on Flexible Film Thermoelectric Module

[1]*Vasyl Stefanyk Precarpathian National University, Ivano-Frankivsk, Ukraine, bdzundza@gmail.com*
[2]*Ivano-Frankivsk National Medical University, Ivano-Frankivsk, Ukraine, oksanakostuk@gmail.com*
[3]*Department of Materials Engineering, Ben-Gurion University, Beer-Sheva, Israel dashevsky.45@mail.ru*

Thermal detectors find a significant niche in the market of modern sensors. $Bi_2T_3$ and $PbTe$ semiconductors are effective thermoelectrics and excellent candidates for different applications. In the present work, a technology for fabrication of the thermal detector based on high-efficient $p$-$Bi_{0.5}Sb_{1.5}Te_3$ and $n$-$PbTe$ films on thin flexible polyimide substrate has been developed. The preparation of films was performed by a flash evaporation method. The high sensitivity of the devices is obtained as a result of the high Seebeck coefficient and low value of thermal conductivity for thin thermoelectric films. The devices operate in the Johnson-Nyquist noise limit of the thermocouple. The high performance enables fast and sensitive detection of low levels of thermal power and infrared radiation at room temperature.

**Keywords**: $Bi_2Te_3$, $PbTe$, thermal detectors, thermoelectric properties, thin films.

*Received 30 January 2021; Accepted 10 February 2021.*

## Introduction

Thermal detectors find a significant niche in the market of modern sensors [1, 2]. Many existing and new applications require accurate measurement of heat fluxes. Thermoelectric converters (modules) are widely used for cooling (Peltier effect) or generation of energy (Peltier and Seebeck effects) [3-6]. Seebeck effect, which is the physical basis for the thermal thermoelectric detectors. Recently, interest in the use of thermoelectric devices as thermal detectors is very actual. Thermoelectric detectors are used also to measure laser power from a few microwatts to several watts [7].

The $p$-type $Bi_2Te_3$ based compounds and $n$-type $PbTe$ are the most effective thermoelectric materials [8-13]. Thin films have a big potential for application in thermal thermoelectric detectors due to their small thickness, which allowed them to have the large number of thermocouples in a volume unit [14]. These films were fabricated by co-evaporation, molecular beam epitaxy, hot wall, magnetron sputtering, pulsed laser deposition [15-20, Taras Parashchuk, Leonid Chernyak, Sergey Nemov, Zinovi Dashevsky, Influence of Deformation on $Pb_{1-x}In_xTe_{1-y}I_y$ and $Pb_{1-x-y}Sn_xIn_yTe$ Films, 257(12), 2000304]. However, the high value of the figure of merit $Z$ for $Bi_2Te_3$-based films like for bulk crystals ($Z \sim 3 \times 10^{-3}$ $K^{-1}$) [20-22] had been not achievable for a long time. Recently, the high value of $Z \approx 3 \times 10^{-3}$ $K^{-1}$ at $T = 300$ K for $p$-type $Bi_{0.5}Sb_{1.5}Te_3$ films was obtained by Professor Z. Dashevsky with co-authors in 2020 [24].

For the film preparation, an ultrathin polyimide substrate with a thickness of ~ 3 μm was used aiming to minimize the negative heat wastes. The benefits of polyimide material are the extremely low thermal conductivity (~3.5 $Wcm^{-1}K^{-1}$) and high flexibility. The use of a flexible polyimide substrate and perforation cuts between $p$-and $n$-legs allowed us to develop a compact (packaged) design of Film Thermoelectric Module (FTEM). Based on this FTEM, a thermal thermoelectric detector was proposed.

## I. Experimental procedure

Synthesis of $Bi_{0.5}Sb_{1.5}Te_3$ and $PbTe$ doped by In or I

O. Kostyuk, Ya. Yavorsky, B. Dzundza, Z. Dashevsky
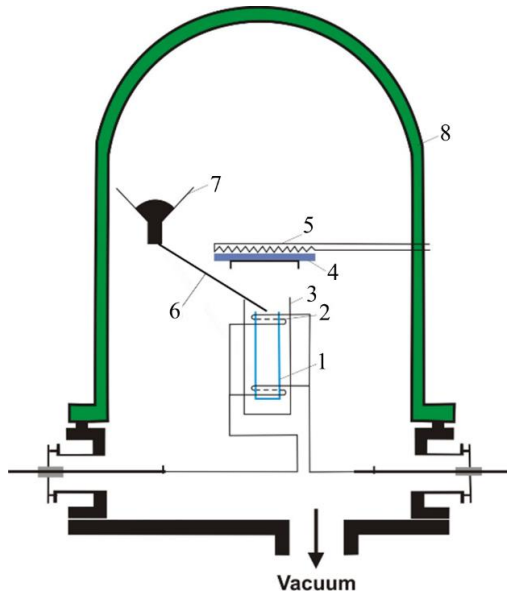
**Fig. 1.** Schematic view of flash evaporation. 1 - quartz crucible, 2 - crucible heater, 3 - heat shield, 4 - substrate, 5 - substrate heater, 6 - channel, 7-powder vessel, 8 - vacuum chamber.

was carried out by direct melting of components for 10 hours at 1073 K (for $Bi_{0.5}Sb_{1.5}Te_3$ based alloys) and at 1273 K (for PbTe doped by In or I) in sealed quartz ampoules evacuated to a residual pressure of $10^{-5}$ mbar. Then each ampoule was taken from the furnace and quenched into cold water. High purity initial components for the synthesis have been used. The resultant ingots were crushed into fine powders by ball milling in an argon atmosphere. The lower concentration of the $Bi_{0.5}Sb_{1.5}Te_3$ composition was obtained by introducing over stochiometric Te (1 - 3 wt. %) due to the compensation effect of metal vacancies [8]. The preparation of PbTe with different electron concentration has been performed using donor dopant (In or I) [9, 25].

The $p$-$Bi_{0.5}Sb_{1.5}Te_3$ and $n$-PbTe:In (I) films were deposited by flash evaporation technology [24]. A set up for obtaining films by flash evaporation method is shown in Fig. 1. For film preparation, $Bi_{0.5}Sb_{1.5}Te_3$ or PbTe : In(I) powder was introduced into the preheated quartz crossable 1 from a mechanically vibrated powder vessel 7. The evaporator is a quartz crossable 1 with a molybdenum wire heater 2, surrounded by a molybdenum heat screen 3. The powdered material is introduced to the crucible from the powder vessel 7 through a water-cooled channel 6. The heating of the substrate is received by substrate heater 5. All parts of the device are located in chamber 8 under a vacuum of $10^{-5}$ mbar. The temperature of the substrate for film preparation was $T_s = 523 - 573$ K; evaporation velocity was $v_e = 0.1$ μm/min. After the evaporation process, all films were annealed at the same evaporation chamber at $T_t = 623$ K for 0.5 h at the atmosphere of pure argon with the pressure of $p = 0.9$ atm.

The plasma-chemical method of cyclohexane $C_6H_{12}$ polymerization was applied to fabricate insulation (polymeric) cover with a thickness of ~ 0.5 μm for the protective coating of film thermoelectric legs.
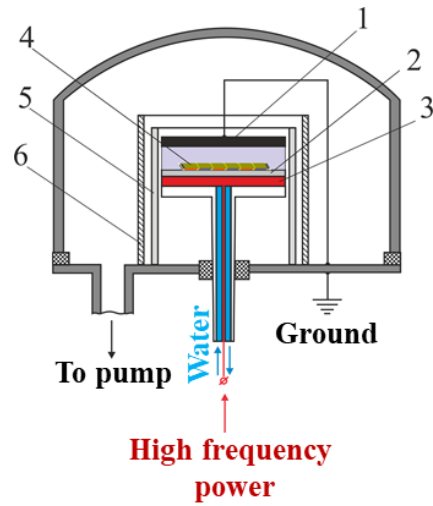


**Fig. 2.** Schematic view of a reactor for the fabrication of a thin polymeric layer. 1 – upper electrode, 2 – quartz plate, 3 – lower electrode, 4 – film thermoelectric module, 5 – quartz cup; 6 – screen.

Polymerization of gas was carried out in high-frequency plasma ($f$ ~14 mHz). The schematic view of the reactor for the fabrication of a thin polymeric layer is shown in Fig. 2. The reactor was placed in a high vacuumed chamber. In the reactor, the discharge was ignited between electrodes 1 and 3 with a diameter of 100 mm. The distance between the electrodes was 25 mm. The upper electrode was grounded. RF power was supplied to the lower electrode. The FTEM was located on this electrode on the surface of a quartz plate with a diameter of 100 mm. The discharge area was limited by screen 5 with a diameter of 150 mm. The vapor pressure of cyclohexane gas was 1 Torr. The manufactured insulating layer is characterized by high breakdown voltage ($E$ ~$10^5$ V/mm), high continuity, and chemical resistance.

The structural analyses of the films were investigated by the X-ray diffraction method. All details of the XRD-analysis are discussed in ref. [24].

For the investigation of the transport properties on thin films (Seebeck coefficient $S$, electrical conductivity $\sigma$) the unique measurement setup has been used [24]. The accuracy of the temperature measurement was 0.1 - 0.2 K, and of the magnetic field ± 3 %. The uncertainty of the Seebeck coefficient and electrical conductivity measurements was 2 %.

The investigation of the heat transfer (thermal diffusivity) at thin films, based on the effect that the sample is excited by two mutually interfering laser beams and described in [26]. The uncertainty of the thermal diffusivity measurements was ~ 8 %. The total thermal conductivity was calculated using the following formula:

$$\kappa = \alpha \rho c_p, \tag{1}$$
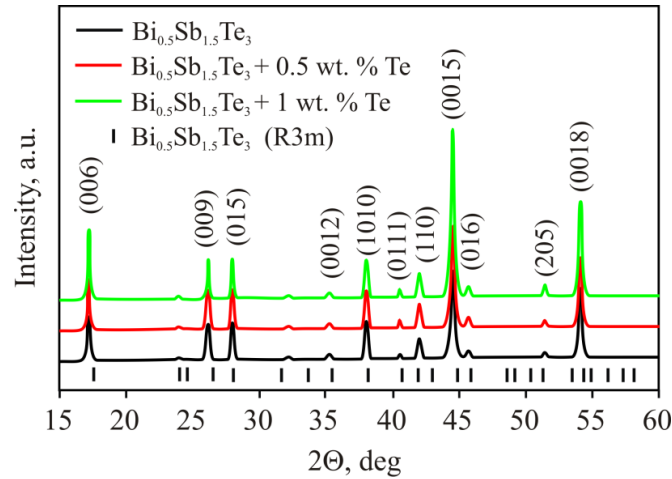
**Fig. 3.** XRD patterns of $Bi_{0.5}Sb_{1.5}Te_3$ based films on a polyimide substrate.
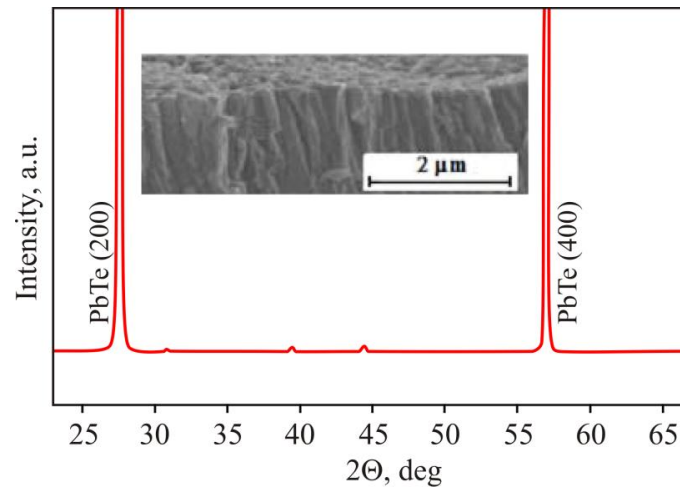


**Fig. 4.** XRD spectra of PbTe:In films on a polyimide substrate. The inset shows the high-resolution SEM image of the cross-section of the PbTe:In film.

where $\rho$ is the single crystal density, and $c_p$ was estimated within the Dulong-Petit limit.

## II. Results and discussion

### 2.1. Structural properties

The quality of $Bi_{0.5}Sb_{1.5}Te_3$ films was controlled using the XRD analysis. Figure 3 shows the XRD-patterns for these films on the amorphous (polyimide substrate). The substrate temperature for film preparation was $T_s = 523$ K. The sharp reflections of the XRD-patterns indicate the polycrystalline nature of the investigated films.

PbTe films had a column-like microstructure with the orientation of the columns nearly perpendicular to the substrate plane (see the insert in Fig. 4). The grain height corresponds to the film thickness (about 3 μm), and the column diameter determined from AFM images we associate with the grain size. At $T_s = 523$ K, the nanocrystalline films with a grain size of about 300 nm were prepared (Figure 4).

### 2.2. Thermoelectric properties

All $p$-type ($Bi_{0.5}Sb_{1.5}Te + 0.5$ wt. % Te and $Bi_{0.5}Sb_{1.5}Te + 1.0$ wt. % Te) and $n$-type ($Pb_{0.9995}In_{0.0005}Te$. and $PbTe_{0.9996}I_{0.0004}$) films were prepared on a thin flexible polyimide substrate with a thickness of ~ 5 μm.
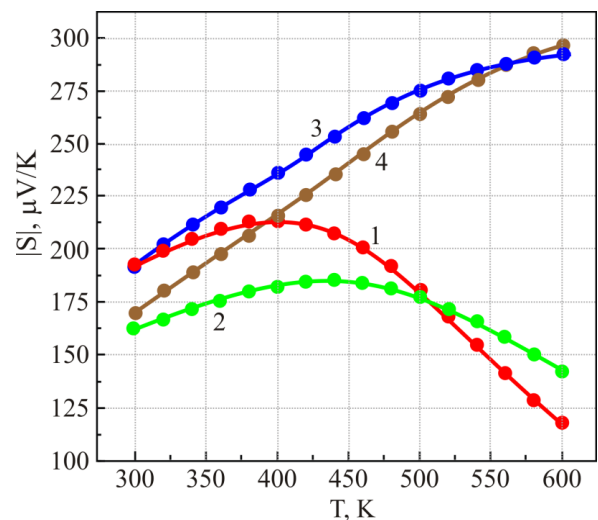


**Fig 5.** Absolute value of Seebeck cofficient $S$ as a function of temperature for $p$-and $n$-type thermoelectrtic films. 1. $p$-type $Bi_{0.5}Sb_{1.5}Te + 1.0$ wt. % Te. 2. - $p$-type $Bi_{0.5}Sb_{1.5}Te + 0.5$ wt. % Te. 3. - $n$-type $Pb_{0.9995}In_{0.0005}Te$. 4 - $PbTe_{0.9996}I_{0.0004}$.

Figure 5 represents the Seebeck coefficient $S$ for

$Z$ value for $p$-$Bi_{0.5}Sb_{1.5}Te_3$ bulk samples [21, 23].
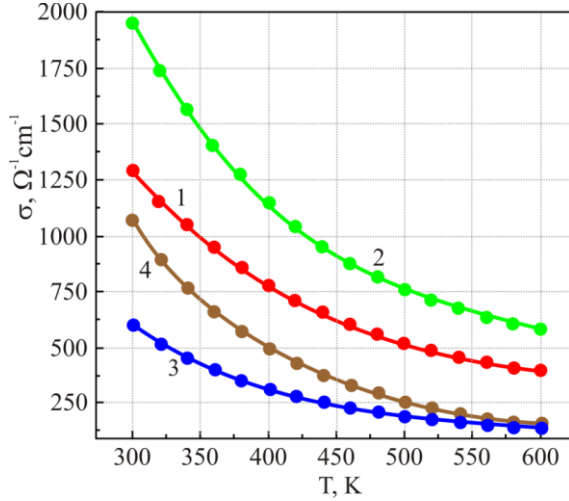


**Fig. 6.** Electrical conductivity s as a function of temperature for $p$-and $n$-type thermoelectric films. 1. $p$-type $Bi_{0.5}Sb_{1.5}Te$ + 1.0 wt. % Te. 2. - $p$-type $Bi_{0.5}Sb_{1.5}Te$ + 0.5 wt. % Te. 3. - $n$-type $Pb_{0.9995}In_{0.0005}Te$. 4 - $PbTe_{0.9996}I_{0.0004}$.
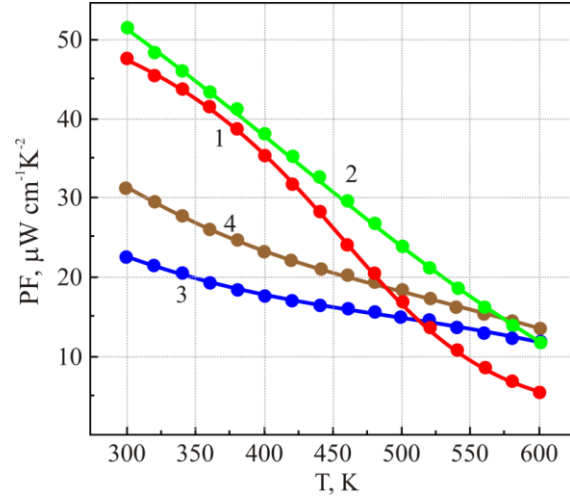


**Fig. 7.** Power factor $P = S^2$s as a function of temperature for $p$-and $n$-type thermoelectric films. 1. $p$-type $Bi_{0.5}Sb_{1.5}Te$ + 1.0 wt. % Te. 2. - $p$-type $Bi_{0.5}Sb_{1.5}Te$ + 0.5 wt. % Te. 3. - $n$-type $Pb_{0.9995}In_{0.0005}Te$. 4 - $PbTe_{0.9996}I_{0.0004}$.

these films over the entire temperature range of 300 - 600 K. The temperature trend of the Seebeck coefficient for $p$-type films shows the maximum and then goes down due to the effect of the intrinsic carriers, which is typical for narrow-band semiconductors.

The electrical conductivity of the investigated films is decreasing over the investigated temperature range indicating a metallic tendency (Figure 6). The excellent thermoelectric performance of the fabricated films was confirmed by the estimation of the Power Factor $P = S^2\sigma$. (Figure 7). The maximum value of $S^2\sigma \approx 50$ W/cmK at $T = 300$ K for $p$-type films, which is practically equal to the power factor for the best bulk samples with the same chemical composition [19, 21].

Table 1 presents measured thermoelectric properties (Seebeck coefficient $S$, electrical conductivity $\sigma$ and thermal conductivity $\kappa$) at $T = 300$ K for $p$-type and n-type films of different compositions. The figure of merit $Z$ for the film sample with $Bi_{0.5}Sb_{1.5}Te$ + 0.5 wt. % Te composition achieved the value of $Z \approx 3.0 \times 10^{-3}$ K$^{-1}$ at 300 K, which is practically equal to the

## III. Thermal detector on flexible Film Thermoelectric Module (FTEM)

*3.1. Fabrication technology of thermal detector*

The preparation of FTEM includes the following stages:

1. Preparation of $p$-type $Bi_{0.5}Sb_{1.5}Te_3$ film legs with a thickness of ~ 3 μm on both sides of the polyimide substrate (~10 μm).

2. Preparation of $n$-type $PbTe_{0.9996}I_{0.0004}$ film legs with a thickness of ~ 3 μm on both sides of the polyimide substrate.

3. Fabrication of perforations between $p$- and $n$-type legs. The size of the cut is ~ 0.2 mm, and the distance between the cuts is ~ 1 mm.

4. Fabrication of the electrical connection between $p$- and $n$-type legs by metallic layers of Cr with a thickness of 0.1 μm and Au with a thickness of 1 mm) on both

**Table 1**

Thermoelectric properties of $p$-type $Bi_{0.5}Sb_{1.5}Te_3$ and $n$-type PbTe:In(I) films and bulk crystals at $T = 300$ K.

| Composition | Type of material | Seebeck coefficient $S$, μV/K | Electrical conductivity $\sigma$, $\Omega^{-1}cm^{-1}$ | Thermal conductivity $\kappa$, W/cm-K | Figure of merit $Z \times 10^3$, K$^{-1}$ | Ref. |
|---|---|---|---|---|---|---|
| $Bi_{0.5}Sb_{1.5}Te_3$+ 1.0 wt. % Te | film | 190 | 1250 | 15 | 3.0 | |
| $Bi_{0.5}Sb_{1.5}Te_3$ + 0.5 wt. % Te | film | 160 | 2000 | 18 | 2.8 | |
| $Pb_{0.9995}In_{0.0005}Te$ | film | -190 | 670 | 20 | 1.2 | |
| $PbTe_{0.9996}I_{0.0004}$ | film | -160 | 1500 | 23 | 1.7 | |
| $Bi_{0.5}Sb_{1.5}Te_3$ | bulk | 200 | 1150 | 16 | 3.0 | [21, 23] |
| $Pb_{0.9995}In_{0.0005}Te$ | bulk | -200 | 600 | 23 | 1.1 | [26, 27] |

sides of the polyimide substrate and inside the perforation cuts.

5. Fabrication of a thin protective coating with a thickness of ~ 0.5 μm on both sides of the FTEM by the plasma-chemical method of cyclohexane polymerization.

A schematic view of the main stages of fabrication of the flexible FTEM based on $p$-Bi$_{0.5}$Sb$_{1.5}$Te$_3$ and $n$-PbTe thermoelectric materials is shown in Fig. 8.

The flexible polyimide substrate and perforation cuts between $p$-and $n$-legs allow to bend substrate along the perforation and to create a compact (packaged) design of the FTEM. Based on this FTEM, a thermopile detector was developed. This thermopile detector consists of three elements: an absorber, a sensor element (FTEM), and a cooling body to dissipate the incoming heat. As shown in Fig. 9, a thermopile sensor connected to one type of junction (hot junction at temperature $T_h$) is exposed to the absorption area and another type of junction (cold junction at temperature $T_c$) is exposed to the heat sink. Due to the thermoelectric effect, the temperature difference causes an electrical voltage. This output voltage is directly proportional to the power of the incoming radiation.

### 3.2. Calculation of thermal detector characteristics
<u>Rise time</u>

The initial and boundary conditions for such a design of FTED (package) are as follows:

$$T(x, y, z) = T_0, t = 0 . \qquad (2)$$

On the side surfaces at any given time, the heat flux coming from the bulk equals the heat flux emitted into the environment:

$$[-\kappa \frac{\partial T}{\partial x} + 4\varepsilon\sigma_B T_0^3 (T - T_0)]_{x=A} = 0,$$

$$[-\kappa \frac{\partial T}{\partial y} + 4\varepsilon\sigma_B T_0^3 (T - T_0)]_{y=B} = 0,$$

$$(3)$$

$$[-\kappa \frac{\partial T}{\partial x} + 4\varepsilon\sigma_B T_0^3 (T - T_0)]_{x=0} = 0,$$

$$[-\kappa \frac{\partial T}{\partial y} + 4\varepsilon\sigma_B T_0^3 (T - T_0)]_{y=0} = 0,$$

where $\varepsilon$ is the emissivity of the thermoelectric film surface, $A$ and $B$ are the width and thickness of the packet.

On the upper surface with $\varepsilon \approx 1$, the incident heat flux is equal to the algebraic sum of the heat flux radiated from the surface and removed from it into the packet:



**Fig. 8.** Schematic view of FTEM. a) - planar design. b) a view of the film module after the protective coating. 1 - $p$-legs. 2 - $n$-legs. 3 - perforation. 4 - metallic connecting layers between legs. 5 - output electric contacts.
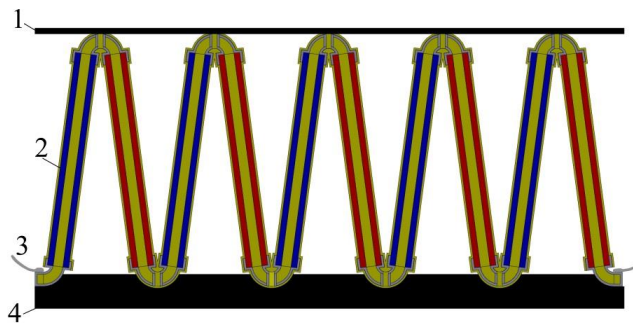


**Fig. 9.** Schematic view of Film Thermoelectric Detector (FTED). 1– absorption layer. 2– FTEM on flexible (polyimide) substrate. 3 – electric contacts. 4 – heat sink (black body).

$$[-\kappa \frac{\partial T}{\partial z} + 4\varepsilon\sigma_B T_0^3 (T - T_0)]_{z=H} = W E_x(t), \qquad (4)$$

where $H$ is the height of the packet, and:

$$E_x(t) = \begin{cases} 1, t > 0, \\ 0, t = 0. \end{cases} \qquad (5)$$

On the lower surface, when the temperature is equal to the ambient temperature taken as the reference point ($T(x, y, 0) = 0$), a solution to the unsteady heat equation will be:

$$\frac{\delta T}{\delta t} = \left( \frac{\kappa_{ef}}{c\rho_{ef}} \right) \cdot \Delta T, \qquad (6)$$

where

$$c\rho_{ef} = \frac{c\rho_f d_f + c\rho_s d_s}{d_f + d_s}. \qquad (7)$$

For the packet sizes $A$, $B \ll \kappa/4\varepsilon\sigma_B T_0^3$ and $H \ll \kappa/4\sigma_B T_0^3$ (for (Bi$_2$Te$_3$ based alloys $\kappa / 4\varepsilon\sigma_B T_0^3 \sim$ 250 - 300 mm) changes in temperature can be described by exponential dependence with a rise time:

$$\tau_r = \frac{c\gamma ABH}{8\varepsilon\sigma_B T_0^3 (A + B)H + \pi^2 / 4\kappa(AB / H)}, \qquad (8)$$

where $c\gamma ABH$ is the packet heat capacity, $8\varepsilon\sigma_B T_0^3 (A + B)H$ and $(\pi^2 / 4)\kappa(AB / H)$ are the heat transfer coefficients due to radiation $G_r$ and thermal conductivity $G_{tc}$, respectively.

In the case where the heat transfer is mainly determined by the process of heat conduction ($G_{tc} \gg G_r$)

$$\tau_r \approx \frac{4}{\pi^2} \frac{c\gamma H^2}{\kappa}. \qquad (9)$$

This parameter does not depend on $\varepsilon$, and also on the thickness of the thermoelectric layer. Figure 10 presents the calculated values of the rise time $\tau$ as a function of height thermoelectric leg $H$ for thermal detector on FTEM with different thicknesses of the $p$-Bi$_{0.5}$Sb$_{1.5}$Te$_3$ and $n$-PbTe:In thermoelectric films.

Sensitivity
Sensitivity is equal to the ratio of the average square
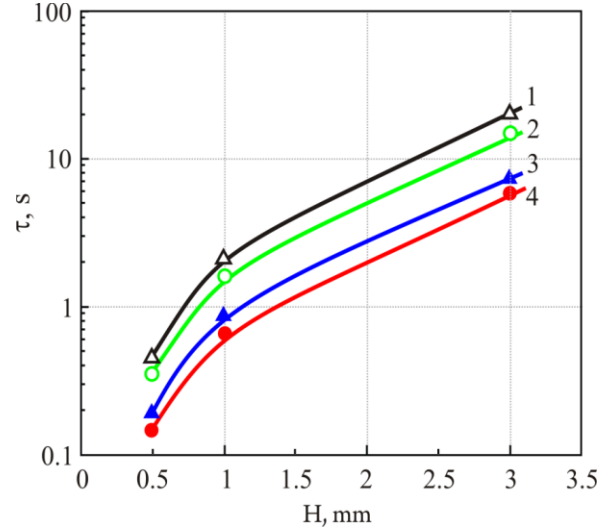


**Fig. 10.** The rise time $\tau$ of thermal detector as a function of thermoelectric leg height $H$. 1- thickness of film leg $d_f = 0.1$ μm. 2 - $d_f = 1$ μm. 3 -$d_f = 5$ μm. 4 - $d_f = 10$ μm.

value of the output signal voltage $V$ measured at the fundamental frequency w (if the incident radiation is modulated with frequency) to the power of the incident radiation $P$:

$$S_s = V/P, \qquad (10)$$

$$V = (S_n + S_p)m, \qquad (11)$$

where $S_n$ and $S_p$ are Seebeck coefficient of $n$- and $p$-legs, $m$ is number of thermocouples.

When the heat transfer from hot junctions to cold junctions is due only to the thermal conductivity of the film thermoelectric legs and the substrate the Eq (11) is converted to the form:

$$P = (k_{efn} + k_{efp})\Delta T m d_f b/l, \qquad (12)$$

where $\kappa_{efn}$ and $\kappa_{efp}$ are effective thermal conductivity of $n$- and $p$-legs, $\Delta T$ is the temperature difference $d_f$ is the film thickness, $b$ and $l$ are the width and length of the thermoelectric legs.

In the case when the radiation flux from the side surface is much smaller than the heat flux along with the packet, the steady spatial temperature distribution in the packet is described by the following expression:

$$T_{(z,\infty)} - T_0 = \frac{W}{4\sigma_Б T_0^2} \frac{\text{sh}[z\sqrt{(8\varepsilon T_0^3 / \kappa)(1 / A + 1 / B)}]}{\text{sh}[H\sqrt{(8\varepsilon\sigma_B T_0^3 / \kappa)(1 / A + 1 / B)}] + \rightarrow} $$
$$\rightarrow + \sqrt{(\varepsilon\kappa / 2\sigma_B T_0^3)(1 / A + 1 / B)}\text{ch}\sqrt{(8\varepsilon\sigma_B T_0^3 / \kappa)(1 / A + 1 / B)}. \qquad (13)$$

Using Eq. (18), we calculated sensitivity $S_s$ as a function of height thermoelectric leg $H$ for a thermal detector with different thicknesses of thermoelectric film legs (Figure 11).
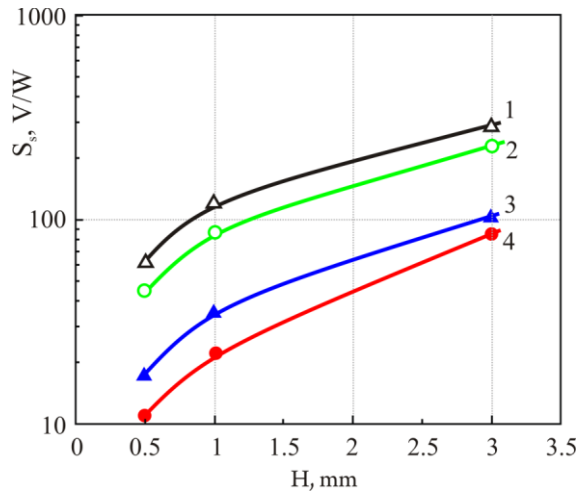
**Fig. 11.** Sensitivity $S_s$ of the thermal detector as a function of thermoelectric leg height $H$. 1- thickness of film leg $d_f = 0.1$ μm. 2 - $d_f = 1$ μm. 3 - $d_f = 5$ μm. 4 - $d_f = 10$ μm.

## Conclusions

In the work, the flexible Film Thermoelectric Module (FTEM), based on $p$-type $B_{2-x}Sb_xTe_3$ and $n$-type PbTe:In (I), on a thin polyimide substrate was developed. The FTEM consists of $p$- and $n$-type thermoelectric films

with a thickness of ~ 3 μm on both sides of the substrate. The parallel electric connection of each type of film on both sides of the substrate and the serial connection of $p$- and $n$-legs by metallic films of Au & Cr were ensured by perforation cuts in the polyimide substrate. The unique design as well as the use of a flexible polyimide substrate allowed us to create a compact (packaged) FTEM.

A thermal thermoelectric detector based on the compact flexible FTEM was developed, which consists of three elements: an absorber, a sensor element (FTEM), and a cooling body to dissipate the incoming heat. The main parameters - rise time and sensitivity of thermal detector were calculated. These characteristics for the optimal design of thermal detector with maximum film thickness and minimal height of FTEM are on a level of best thermoelectric detectors.

***Kostyuk O.*** – PhD, Senior Researcher;
***Yavorsky Ya.*** – PhD, Senior Researcher;
***Dzundza B.*** – PhD, Associate Professor;
***Dashevsky Z.*** – Doctor of Sciences, Professor.

[1]   A. Rogalski, Infrared Detectors (CRC Press, 2010) (https://doi.org/10.1201/b10319).
[2]   A. Rogalski, Prog. Quantum Electron. 27, 59 (2003) (https://doi.org/10.1016/s0079-6727(02)00024-1).
[3]   H.J. Goldsmid, Introduction to thermoelectricity (Springer-Verlag, Berlin, 2016).
[4]   D.M. Rowe, Thermoelectric handbook: Macro to Nano (CRC Press, 2005).
[5]   S. Oualid, F. Kosior, A. Dauscher, C. Candolfi, G. Span, E. Mehmedovic, J. Paris, B. Lenoir, Energy & Environmental Science 13(10), 3579 (2020) (https://doi.org/10.1039/d0ee02579h).
[6]   Z. Dashevsky, The applications of lead chalcogenides in thermoelectric devices. Lead chalcogenides: physics and application. Edited by D. Khokhlov (Talor&Francis, New York, 2003).
[7]   A. Varpula, A.Timofeev, A. Shchepetov, K. Grigoras, J. Hassel, J. Ahopelto, M. Ylilammi, M. Prunnila, Appl. Phys. Lett. 110, 262101 (2017) (https://doi.org/10.1063/1.4989683).
[8]   B.M. Goltsman, B.A. Kudinov, I.A. Smirnov, Semiconductor Thermoelectric Materials Based on $Bi_2Te_3$ (Nauka, Moskow, 1972).
[9]   Yu.I. Ravich, B.A. Efimova, I.A. Smirnov, Semiconducting Lead Chalcogenides (Plenum Press, New York, 1970).
[10] A.P. Goncalves, C. Godart, Alternative strategies for thermoelectric materials development. in New Materials for Thermoelectric Applications: Theory and Experiment edited by V. Zlatic, A. Hewson (Springer, New York, 2013).
[11] J. Herremans, B. Wiendliocha, Tetradymites: $Bi_2Te_3$-related materials, in: C Uher (Ed.), Materials Aspect of Thermoelectricity, (CRS Press, Boca Raton, 2016).
[12] O. Ben-Yehuda, R. Shuker, Y. Gelbstein, Z. Dashevsky, M.P. Dariel, J. Appl. Phys. 101, 113707 (2007) (https://doi.org/10.1063/1.2743816).
[13] I.V. Horichok, T.O. Parashchuk, J. Appl. Phys 127, 055704 (2020) (https://doi.org/10.1063/1.5130747).
[14] B.M. Goltzman, Z.M. Dashevsky, V.I. Kaydanov, N.V. Kolomoetz, Film thermoelements: physics and application (Nauka, Moscow, 1985).
[15] L. Silva, M. Kaviany, C. Uher, J. Appl. Phys. 97, 114903 (2005) (https://doi.org/10.1063/1.1914948).
[16] E. Symeou, M. Pervolaraki, C.N. Mihailescu, at. el., Appl. Surf. Sci. 336, 138 (2015) (https://doi.org/10.1016/j.apsusc.2014.10.038).
[17] D. Bourgault, C.G. Garampon, N. Caillault, L. Carbone, J.A. Aymami, Thin Solid Films 516, 8579 (2008) (https://doi.org/10.1016/j.tsf.2008.06.001).

[18] Z. Dashevsky, A. Belenchuk, O. Shapoval, E. Gartstein, Thin Solid Films. 461, 256 (2004) (https://doi.org/10.1016/j.tsf.2004.01.087).

[19] A. Jdanov, J. Pelleg, Z. Dashevsky, R Shneck, Materials Science and Engineering B. 106, 89 (2004) (https://doi.org/10.1016/j.mseb.2003.09.026).

[20] T. Parashchuk, L. Chernyak, S. Nemov, Z. Dashevsky, Physica Status Solidi (b), 257(12), 2000304 (2020) (https://doi.org/10.1002/pssb.202000304).

[21] Z. Dashevsky and S. Skipidarov. Investigating the Performance of Bismuth - Antimony Telluride in Novcgel Materials and Device Design Concepts// edited by M. Nikitin and S. Skipidarov (Springer, New York, 2019).

[22] R. Deng, X. Su, S. Hao, Z. Zheng, M. Zhang, H. Xie, W. Liu, Y. Yan, C. Wolverton, C. Uher, M.G. Kanatzidis, X. Tang, Energy Environ. Sci 6, 1520 (2018) (https://doi.org/10.1039/c8ee00290h).

[23] I.T. Witting, J.A. Grovogui, V.P. Dravid, G.J. Snyder, J. of Materiomics 6, 532 (2020) (https://doi.org/10.1016/j.jmat.2020.04.001).

[24] T. Parashchuk, O. Kostyuk, L. Nykyruy, Z. Dashevsky, Mater Chem Phys. 253, 123427 (2020) (https://doi.org/10.1016/j.matchemphys.2020.123427).

[25] T. Parashchuk, Z. Dashevsky, K. Wojciechowski, J. Appl. Phys. 125 245103 (2019) (https://doi.org/10.1063/1.5106422).

[26] B. Dzundza, L. Nykyruy, T. Parashchuk, E. Ivakin, Y. Yavorsky, L. Chernyak, Z. Dashevsky, Physica B 588, 412178 (2020) (https://doi.org/10.1016/j.physb.2020.412178).

[27] K. Wojciechowski, T. Parashchuk, B. Wiendlocha, O. Cherniushok, Z. Dashevsky, Journal of Materials Chemistry C, 8, 13270 (2020) (https://doi.org/10.1039/d0tc03067h).

О. Костюк[1,2] Я. Яворський[1], Б. Дзундза[1], З. Дашевський[3]

# Розробка теплового детектора на основі гнучкого плівкового термоелектричного модуля

[1]*Прикарпатський національний університет імені Василя Стефаника, Івано-Франківськ, Україна, bdzundza@gmail.com*
[2]*Івано-Франківський національний медичний університет, Івано-Франківськ, Україна, oksanakostuk@gmail.com*
[3] *Університет Бен-Гуріона, Беер-Шева, Ізраїль, dashevsky.45@mail.ru*

Теплові детектори займають значну нішу на ринку сучасних датчиків. Напівпровідники $Bi_2T_3$ та $PbTe$ є ефективними термоелектриками та чудовими кандидатами для різних застосувань. У цій роботі розроблена технологія виготовлення плівок $p-Bi_{0.5}Sb_{1.5}Te_3$ та $n-PbTe$ з високою термоелектричною ефективністю на тонкій гнучкій поліімідній підкладці. Підготовку плівок проводили методом швидкого випаровування. Висока чутливість приладів обумовлена високим коефіцієнтом Зеебека та низькою теплопровідністю тонкої термоелектричної плівки. Пристрої працюють в межі шуму термопари Джонсона-Найквіста. Продуктивність дозволяє швидко і чутливо виявляти низькі рівні теплової потужності та інфрачервоного випромінювання при кімнатній температурі.

**Ключові слова:** $Bi_2Te_3$, $PbTe$, теплові детектори, термоелектричні властивості, тонкі плівки.